Polydopamine nanocoated whole-cell asymmetric biocatalysts

ChemComm

Accepted Manuscript

This article can be cited before page numbers have been issued, to do this please use: L. Wang, Z. Hu, X. Yang, B. Zhang, W. Geng, G. Van Tendeloo and B. Su, *Chem. Commun.*, 2017, DOI: 10.1039/C7CC01283G.

ROYAL SOCIETY OF CHEMISTRY

rsc.li/chemcomm

View Article Online
DOI: 10.1039/C7CC01283G

Journal Name

COMMUNICATION

Polydopamine Nanocoated Whole-Cell Asymmetric Biocatalyst

Li Wang,[a,b] Zhi-Yi Hu,[c] Xiao-Yu Yang,[a*] Bo-Bo Zhang,[b,d*] Wei Geng,[a] Gustaaf Van Tendeloo,[c,e] and Bao-Lian Su[a,b,*]

Received 00th January 20xx,
Accepted 00th January 20xx

DOI: 10.1039/x0xx00000x

www.rsc.org/

Our whole-cell biocatalyst with a polydopamine nanocoating shows high catalytic activity (5 times better productivity than the native cell) and reusability (84% of the initial yield after 5 batches, 8 times higher than the native cell) in asymmetric reduction. It also integrates with titania, silica, and magnetic nanoparticles for multi-functionalization.

Biocatalytic asymmetric reduction, due to its high enantioselectivity, high environmental friendly, and mild reaction condition, has been considered as a promising approach for chemical, pharmaceutical and fuel production.[1, 2] Whole-cell biocatalysts have attracted increasing interest in recent years and show significant cost-saving by no expensive coenzyme regeneration[3]. However, many critical issues must be addressed for their practical application[4,5], such as fast kinetics, high stability and reusability. Most recently, a cell-in-shell technique[6] has been demonstrated as an advanced protection approach for highly improved stability[7-9] and nano-functions introduction[10-13]. For example, a calcium phosphate nanoshell greatly improves the cell stability for biocatalysis enhancement in oil-water biphrase.[14] A titania oxide nanoshell shows good ability to accelerate the bacterial desulfurizing reaction under UV irradiation.[15] However, there are still rare reports on increased whole-cell catalytic activity through shell engineering. Therefore, it is of great scientific and engineering interest to improve the catalytic activity of a whole-cell, as well as its stability and reusability by the shellization technique.

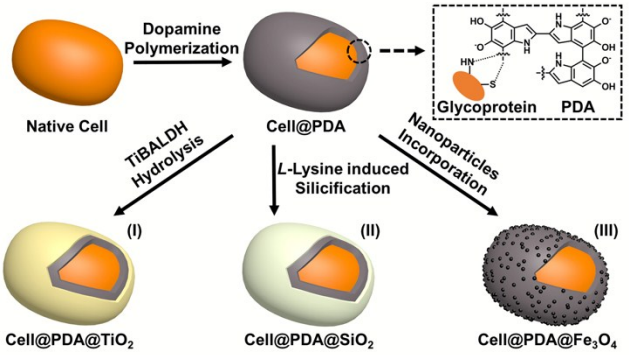

Scheme 1. Schematic diagram of PDA coating and post-functionalization on an individual cell. PDA coating on an individual cell to form cell@PDA, and post-functionalization on cell@PDA to form (I) cell@PDA@TiO_2, (II) cell@PDA@SiO_2, and (III) cell@PDA@Fe_3O_4. Inset image presents the covalent bonding between PDA and glycoproteins in the cell wall.

Polydopamine (PDA) can act as an electron acceptor at neutral and basic pH values because of its functional ligands such as semiquinones and quinones,[16] thus possibly presenting a great prospect in accelerating the transfer of electrons and enhancing catalytic activity during biocatalytic asymmetric reduction. Meanwhile, PDA is a universal adhesion agent[17-19] which can not only coat the cell surface for cell growth control, cell sensing and cell stability increasing in harsh conditions,[20-22] but also easily induce multifunctional nanostructures[23, 24]. We used PDA to coat individual cells to form a cell-in-shell biocatalyst for asymmetric reaction. The biocatalyst presents an enhanced catalytic activity and reusability. Moreover, titania, silica, and iron oxide nanoparticles can be easily introduced around the cell surface by PDA nanocoating to equip the biocatalyst with a high stability in heat and UV conditions and a facile separation during reaction.

Rhodotorula glutinis, a whole-cell biocatalyst with a good yield and an excellent enantiomeric excess (*e.e.*) for production of chiral alcohol,[25] was used to incorporate with PDA nanocoating. The synthetic route for the cell in PDA nanocoating (Cell@PDA) biocatalyst is illustrated in Scheme 1. PDA nanocoating is formed by pH triggered, oxidative

[a] *State Key Laboratory of Advanced Technology for Materials Synthesis and Processing, Wuhan University of Technology, 122 Luoshi Road, 430074 Wuhan, China. Email: xyyang@whut.edu.cn, baoliansu@whut.edu.cn*
[b] *Laboratory of Inorganic Materials Chemistry (CMI), University of Namur, 61 Rue de Bruxelles, B-5000 Namur, Belgium. Email: bao-lian.su@unamur.be*
[c] *EMAT (Electron Microscopy for Materials Science), University of Antwerp, Groenenborgerlaan 171, B-2020 Antwerp, Belgium.*
[d] *Key Laboratory of Industrial Biotechnology, Ministry of Education, School of Biotechnology, Jiangnan University, 214122 Wuxi, China. Email: superzbobo@gmail.com*
[e] *Nanostructure Research Centre, Wuhan University of Technology, 122 Luoshi Road, 430074 Wuhan, China.*
Electronic Supplementary Information (ESI) available: [details of any supplementary information available should be included here]. See DOI: 10.1039/x0xx00000x

polymerization of dopamine monomers (Figure S1), adherence on the cell wall via self-assembly between PDA and amine or thiol groups of glycoprotein (Inset image in Scheme 1). Cell@PDA can be functionalized by an additional layer linked with catechol or imino groups in PDA via various approaches. (I) Catechol groups and imino groups of PDA can facilitate a nucleophilic attack on the center of Titanium(IV) bis(ammonium lactato) dihydroxide (TiBALDH), leading to hydrolysis and condensation to form an titania functional layer around the cell in PDA nanocoating (Cell@PDA@TiO_2). (II) Carboxyl groups of PDA can graft *L*-lysine, subsequently inducing silicification on the coating surface to form a silica functional layer around the cell in PDA nanocoating (Cell@PDA@SiO_2). (III) Carboxylic acid functionalized magnetic iron oxide nanoparticles can be decorated on the PDA nanocoating through binding between carboxyl groups and catechol groups for functionalizing the cell with magnetism (Cell@PDA@Fe_3O_4).

Scanning electron microscopy (SEM) demonstrates the morphology of the native cells (Figure 1a) and cell@PDA (Figure 1b), respectively. Compared with the native cell, the cell@PDA presents a clear nanocoating which leads to an increased roughness of the surface. The presence of the PDA nanocoating is also evidenced by a color change of the harvested cells from orange to deep brown (Figure S2). The PDA coating shows opaque to visible light due to its highly conjugated aromatic rings. Transmission electron microscopy (TEM) displays the cross-section structure of the native cell (Inset in Figure 1c) and the cell@PDA (Inset in Figure 1d), revealing the cell wall (Figure 1c) in the native cell surface and the PDA nanocoating (Figure 1d) in the cell@PDA. The PDA nanocoating affects the growth kinetics of cells as monitored photospectrometrically by increasing the lag time (Figure S3a), although the growth rates of the native cell and the cell@PDA are similar after starting of the growth (Figure S3b). Live/dead viability probes, consisting of a FUN1 viability indicator and the counterstain Calcofluor WhiteM2R, were used to test cells viability. When a cell culture is incubated in a medium containing these probes, the metabolically active cells can process the cell-diffusely green-fluorescent FUN1 dye to mark their intravacuolar structures as red-fluorescent spots, indicative of living cells, whereas the cell walls can be stained as fluorescent-blue rings by Calcofluor WhiteM2R, regardless of the cells metabolic state. Confocal laser scanning microscopy (CLSM) on suspensions of the probe-stained native cell (Figure 1e) and cell@PDA (Figure 1f) confirms that the percentage of living cells is close to 100%. (Table S1)

Cell@PDA was applied in an asymmetric reduction as shown in Figure S4. Biocatalytic activities of the native cell and the cell@PDA have been illustrated in Figure 1e and Table S2. The product *e.e.* was consistently above 99%, indicating a great enantioselectivity of both cells. The native cells displayed a product yield increase during the whole catalytic period (0-24 h) with the yield reaching 39.7% after 24 h reaction and a productivity (0-24 h) of 0.017 mmol/L/h. The cell@PDA presented a product yield increase during 0-9 h and then maintained a plateau. The highest yield of the cell@PDA

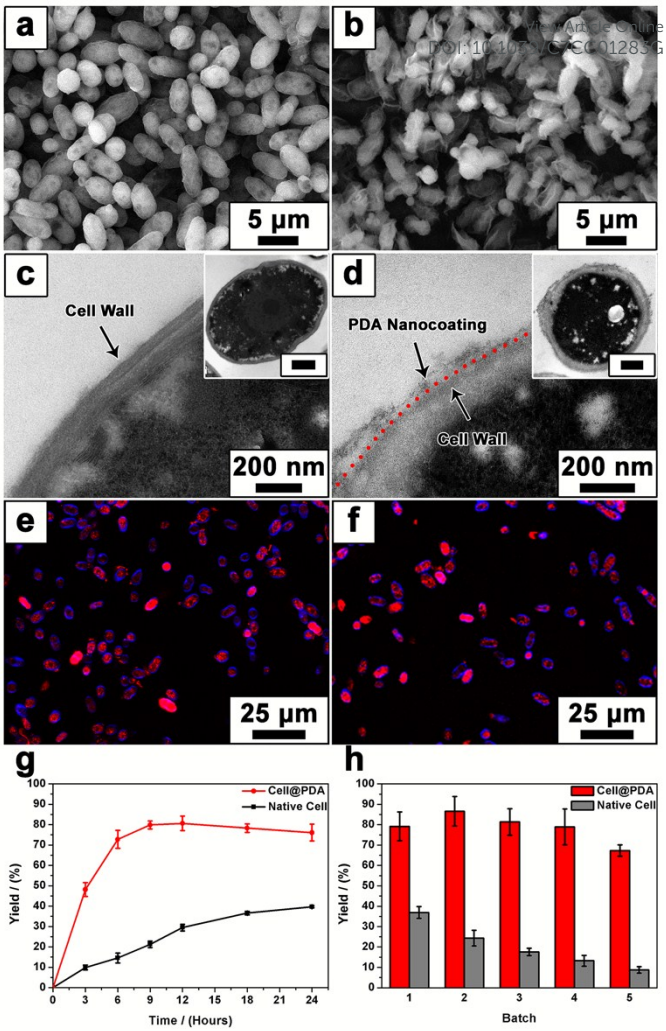

Figure 1. Nanostructure, viability and biocatalytic activity of the native cell and cell@PDA. (a) SEM micrograph of the native cells. (b) SEM micrograph of cell@PDA. (c) TEM micrographs of a native cell (Inset image, scale bar represents 1 μm) and the cell surface. (d) TEM micrographs of cell@PDA (Inset Image, scale bar represents 500 nm) and the surface. The interface between the cell wall and the PDA nanocoating is highlighted by a red dotted line. (e) CLSM micrograph of the fluorescent probes testing for the native cell. (f) CLSM micrograph of the fluorescent probes testing for cell@PDA. Red spots imply that the cells are alive. Cell walls are stained fluorescent blue. (g) (*S*)-1-phenylethanol yield of the native cell and cell@PDA as a function of time. Error bars indicate standard deviations over three independent reactions. (h) Recycling (*S*)-1-phenylethanol yield of the native cell and cell@PDA. Error bars indicate standard deviations over three independent reactions.

showed 79.8% which is twice as large as the one of the native cell. The productivity of the cell@PDA (0-9 h) was calculated to be 0.089 mmmol/L/h, which is 5 times higher than that of the native cell. Consequently, a PDA shell significantly improves the efficiency of the asymmetric reduction catalyzed by the whole-cell. Note (Table S2) that PDA cannot catalyze the asymmetric reduction. However, abundant catechol groups in PDA, the redox-active functional ligands, could act as a redox shuttle for the transfer of two protons and two electrons[16], thus accelerating the rate of electron transfer in the biocatalytic asymmetric reduction or from cytoplasm to extracellular environment[26] for enhancing cell catalytic activity. The asymmetric reduction recycling of the native cell and

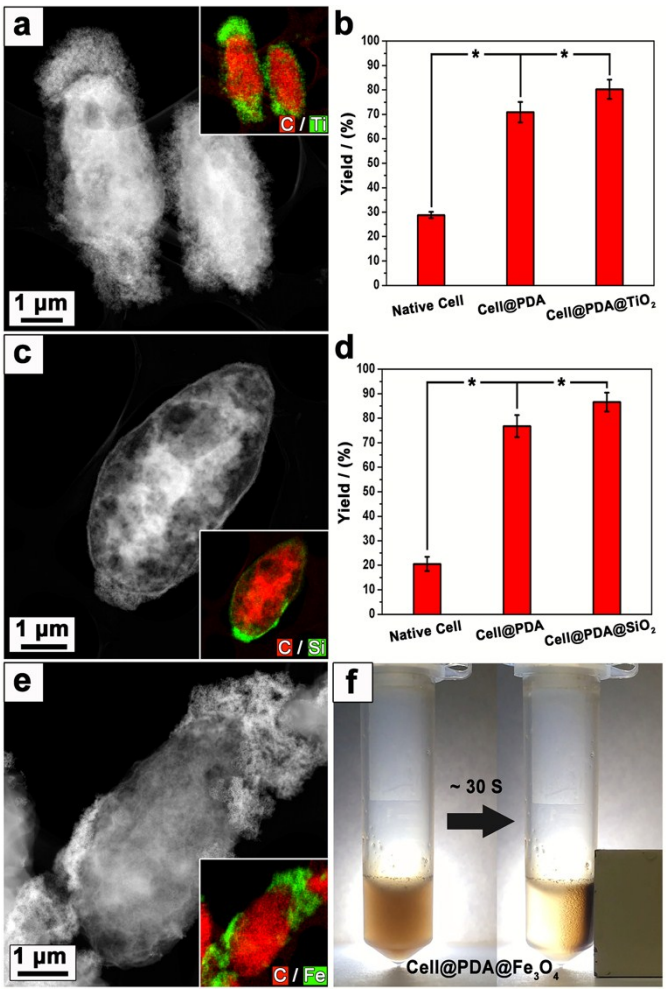

Figure 2. Post-functionalization on cell@PDA. (a) HAADF-STEM image and the corresponding EDX elemental mapping (inset, C: red, Ti: green) of cell@PDA@TiO_2. (b) 24 h (*S*)-1-phenylethanol yield of the native cell, cell@PDA, and cell@PDA@TiO_2 after 4 h UV light treatment. Error bars indicate standard deviations over three independent reactions. *Significant different from the native cell, cell@PDA, and cell@PDA@TiO_2 for product yield at $p < 0.05$ (ANOVA). (c) HAADF-STEM image and the corresponding EDX elemental mapping (inset, C: red, Si: green) of cell@PDA@SiO_2. (d) 24 h (*S*)-1-phenylethanol yield of the native cell, cell@PDA, and cell@PDA@SiO_2 after 1 h 45°C water bath. Error bars indicate standard deviations over three independent reactions. *Significant different from the native cell, cell@PDA, and cell@PDA@SiO_2 for product yield at $p < 0.05$ (ANOVA). (e) HAADF-STEM image and the corresponding EDX elemental mapping (inset, C: red, Fe: green) of cell@PDA@Fe_3O_4. (f) Magnetic behavior of cell@PDA@Fe_3O_4.

cell@PDA was also investigated and the result is shown in Figure 1f. The native cell shows low reusability; the yield decreases with recycling run number and only retains 7.9% after 5 batches. However, the cell@PDA presents a superior retention of its activity; the high yield maintains its initial activity with batch 1-4. Even though it decreased slightly into 67.3% in batch 5, it was still 84% of the initial yield and 8 times higher than the one in the native cell. This result demonstrates that PDA nanocoating not only can enhance the catalytic efficiency of the cell, but also stabilize the high catalytic activity of the cell for increased reusability.

PDA nanocoating can work as a platform for multifunctionalization for the stability enhancement and separation facility of biocatalysts, thus demonstrating a great technological importance in biocatalytic industry. Titania with its ability to absorb UV light can be applied for the protection of entrapped cells under UV irradiation.[15] Introduction of a titania layer on cell@PDA was evidenced by SEM (Figure S5a), TEM (Figure S5d), high angle annular dark field scanning transmission electron microscopy HAADF-STEM (Figure 2a, Figure S6a) and energy dispersive X-ray spectroscopy (EDX) (Figure 2a inset, Figure S5a inset, Figure S6b-e), showing a rough layer of TiO_2 particles on the surface of the cell@PDA. The coating materials, TiO_2 particles synthesized by PDA-induced TiBALDH hydrolysis and condensation (PDA-TiO_2), were further characterized with X-ray diffraction (XRD), indicative of an anatase phase (Figure S7), and presents an enhanced UV absorption around 375 nm and a blue shift around 277 nm, thus providing the encapsulated cell with an improved UV protection (Figure S8). The native cells were set as a control group to be tested by EDX. The result indicates no or less presence of Ti, Si, Fe elements in the native cells. (Figure S9) The cell@PDA@TiO_2 displays a high yield with 84.3% after 24 h normal reaction (Figure S10) with a high viability (Table S1) and a proliferation ability in culture medium (Figure S3). After 24 h bioreduction with 4 h UV treatment, the cell@PDA@TiO_2 presents a yield as high as 80.2% (Figure 2b), while the cell@PDA biocatalyst shows 70.9% (Figure 2b), which strongly proves the UV-protective ability of the PDA@TiO_2 shell. However, the native cell displays a low yield with 28.8% (Figure 2b), because of the intervention of UV light on the cell activity. Silica is an excellent thermal stable material which has been used for cell encapsulation to enhance cell stability under heat conditions.[27] A cell@PDA@SiO_2 was prepared and the homogeneous distribution of silica particles, coated on the surface, was confirmed by SEM (Figure S5b), TEM (Figure S5e), HAADF-STEM (Figure 2c, Figure S11a) and EDX (Figure 2c inset, Figure S5b inset, Figure S11b-e) similarly. The viability and proliferation were evidenced by fluorescent probe testing (Table S1) and growth curve (Figure S3). This biocatalyst demonstrates a yield with 81.7% (Figure S10) after 24 h normal reaction and 86.6% (Figure 2d) after 24 h reaction with 1 h 45 °C water bath treatment. Thanks to the protection of the PDA nanocoating, the cell@PDA presents yield of 76.8% (Figure 2d). As 45 °C could lead to deformation of proteins in the native cell, the yield of the native cell decreased to 20.5% (Figure 2d). Introduction of magnetism on living cells by cell encapsulation can facilitate cell separation[28], which can efficiently decrease the harvesting cost during reaction. The SEM (Figure S5c), TEM (Figure S5f), HAADF-STEM images (Figure 2e, Figure S12a) reveal the morphology of the Cell@PDA@Fe_3O_4 sample, and the corresponding EDX results (Figure 2e inset, Figure S5c inset, Figure S12b-e) demonstrate the presence of Fe_3O_4 particles onto the surface, although the Fe_3O_4 nanocrystals did not form a uniform layer due to their relatively high crystalline degree meaning few defects and/or the less surface groups. The cell@PDA@Fe_3O_4 presents high viability (Table S1), proliferation ability (Figure S3), and a high yield of 67.8% after 24 h reaction (Figure S10), indicating that the incorporation of iron oxide nanoparticles does not heavily hamper the metabolic activity of the cells. The magnetization of the native

cells, the cell@PDA and the cell@PDA@Fe_3O_4 have been characterized quantitatively. As displayed in the magnetic hysteresis curves (Figure S13), the cell@PDA@Fe_3O_4 presents paramagnetic, while the cell and the cell@PDA show diamagnetic, thus confirming that the magnetic properties have been successfully introduced on cell@PDA by the post-functionalization. On the basis of the magnetic properties, the cell@PDA@Fe_3O_4 can be easily and quickly separated from solution in 30 seconds by an external magnetic force (Figure 2f).

In summary, PDA nanocoating greatly enhances the whole-cell asymmetric reductive activity and reusability. The multiple nanoshells composed by titania, silica and iron oxide nanoparticles further provide the cells with a high stability in harsh conditions and a facile separation from the reaction system. Our hybrid nanocoating exhibits a significant improvement of the original cellular in term of biocatalytic activity, reusability and stability, thus giving a pioneering inspiration of cell-in-shell for their application in biocatalytic asymmetric synthesis industry.

This work was supported by PCSIRT (IRT_15R52), NSFC (U1663225, U1662134, 51472190, 51611530672, 51503166), ISTCP (2015DFE52870), HPNSF (2016CFA033), CNPC (PPC2016007) and China Scholarship Council (CSC). We thank Prof. Damien Hermand (URPhyM in UNamur) for cell culture help, Ms. Nöelle Ninane (Narilis in UNamur) for CLSM characterization help and Ms. Siming Wu (WHUT) for magnetic properties characterization help.

Notes and references

1 A. Schmid, J. S. Dordick, B. Hauer, A. Kiener, M. Wubbolts and B. Witholt, *Nature*, 2001, **409**, 258-268.
2 T. Matsuda, R. Yamanaka and K. Nakamura, *Tetrahedron: Asymmetry*, 2009, **20**, 513-557.
3 H. Zhao and W. A. van der Donk, *Curr. Opin. Biotechnol.*, 2003, **14**, 583-589.
4 N. J. Turner, *Nat Chem Biol*, 2009, **5**, 567-573.
5 X. Y. Yang, Z. Q. Li, B. Liu, A. Klein-Hofmann, G. Tian, Y. F. Feng, Y. Ding, D. S. Su and F. S. Xiao, *Adv. Mater.*, 2006, **18**, 410-414.
6 J. H. Park, D. Hong, J. Lee and I. S. Choi, *Acc. Chem. Res.*, 2016, **49**, 792-800.
7 X. Y. Yang, Y. Li, G. Van Tendeloo, F. S. Xiao, and B. L. Su, *Adv. Mater.*, **21**, 1368-1372.
8 N. Jiang, X. Y. Yang, Z. Deng, L. Wang, Z. Y. Hu, G. Tian, G. L. Ying, L. Shen, M. X. Zhang and B. L. Su, *Small*, 2015, **11**, 2003-2010.
9 N. Jiang, X. Y. Yang, G. L. Ying, L. Shen, J. Liu, W. Geng, L. J. Dai, S. Y. Liu, J. Cao, G. Tian, T. L. Sun, S. P. Li and B. L. Su, *Chem. Sci.*, 2015, **6**, 486-491.
10 R. F. Fakhrullin, A. I. Zamaleeva, R. T. Minullina, S. A. Konnova and V. N. Paunov, *Chem. Soc. Rev.*, 2012, **41**, 4189-4206.
11 I. Drachuk, M. K. Gupta and V. V. Tsukruk, *Adv. Funct. Mater.*, 2013, **23**, 4437-4453.
12 M. H. Sun, S. Z. Huang, L. H. Chen, Y. Li, X. Y. Yang, Z. Y. Yuan, and B. L. Su, *Chem. Soc. Rev.*, 2016, **45**, 3479-3563.
13 X. Y. Yang, L. H. Chen, Y. Li, J. C. Rooke, C. Sanchez, and B. L. Su, *Chem. Soc. Rev.*, 2017, **46**, 481-558.
14 Z. Chen, H. Ji, C. Zhao, E. Ju, J. Ren and X. Qu, *Angew. Chem. Int. Ed.*, 2015, **54**, 4904-4908.
15 N. Jiang, G. L. Ying, S. Y. Liu, L. Shen, J. Hu, L. J. Dai, X. Y. Yang, G. Tian and B. L. Su, *Chem. Commun.*, 2014, **50**, 15407-15410.
16 J. H. Kim, M. Lee and C. B. Park, *Angew. Chem. Int. Ed.*, 2014, **53**, 6364-6368.
17 H. Lee, S. M. Dellatore, W. M. Miller and P. B. Messersmith, *Science*, 2007, **318**, 426.
18 S. Hong, Y. S. Na, S. Choi, I. T. Song, W. Y. Kim and H. Lee, *Adv. Funct. Mater.*, 2012, **22**, 4711-4717.
19 Y. Liu, K. Ai and L. Lu, *Chem. Rev.*, 2014, **114**, 5057-5115.
20 S. H. Yang, S. M. Kang, K. B. Lee, T. D. Chung, H. Lee and I. S. Choi, *J. Am. Chem. Soc.*, 2011, **133**, 2795-2797.
21 J. Y. Kim, B. S. Lee, J. Choi, B. J. Kim, J. Y. Choi, S. M. Kang, S. H. Yang and I. S. Choi, *Angew. Chem. In Ed.,* 2016, **55**, 15306-15309.
22 B. Zhang, Z. Sun, Y. Bai, H. Zhuang, D. Ge, W. Shi and Y. Sun, *RSC Adv.*, 2016, **6**, 78378-78384.
23 J. H. Waite, *Nat. Mater.*, 2008, **7**, 8-9.
24 S. M. Kang, N. S. Hwang, J. Yeom, S. Y. Park, P. B. Messersmith, I. S. Choi, R. Langer, D. G. Anderson and H. Lee, *Adv. Funct. Mater.*, 2012, **22**, 2949-2955.
25 E. B. Kurbanoglu, K. Zilbeyaz, M. Ozdal, M. Taskin and N. I. Kurbanoglu, *Bioresour. Technol.*, 2010, **101**, 3825-3829.
26 X. Y. Yang, T. Ge, N. Jiang and B. L. Su, *Energy Environ. Sci.*, 2012, **5**, 5540-5563.
27 G. Wang, L. Wang, P. Liu, Y. Yan, X. Xu and R. Tang, *ChemBioChem*, 2010, **11**, 2368-2373.
28 M. Martín, F. Carmona, R. Cuesta, D. Rondón, N. Gálvez and J. M. Domínguez-Vera, *Adv. Funct. Mater.*, 2014, **24**, 3489-3493.

View Article Online
DOI: 10.1039/C7CC01283G

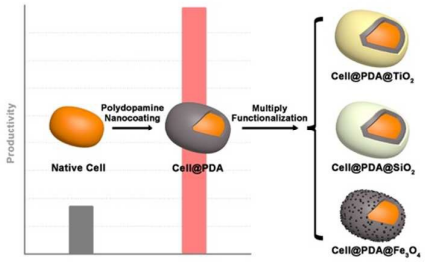

Our whole-cell biocatalyst with a polydopamine nanocoating shows high catalytic activity, reusability and accessibility for multi-functionalization.